Available online at www.sciencedirect.com
ScienceDirect
Geochimica et Cosmochimica Acta 70 (2006) 4380–4391
Geochimica
www.elsevier.com/locate/gca

Basal plane reactivity of phyllosilicates studied in situ by hydrothermal atomic force microscopy (HAFM)

Kirill Aldushin, Guntram Jordan *, Wolfgang W. Schmahl

Dept. für Geo- und Umweltwissenschaften, Sektion Kristallographie, Ludwig-Maximilians-Universität, Theresienstr. 41, 80333 München, Germany

Received 19 September 2005; accepted in revised form 10 April 2006

Abstract

The basal plane reactivities of the sheet silicates apophyllite and phlogopite have been studied by hydrothermal atomic force microscopy (HAFM) in situ in aqueous solutions at temperatures from 20 to 140 °C. At pH 4–5.6 ($T = 20$–100 °C), the apophyllite basal surface undergoes a swelling process which forms square hillocks on the surface. The reaction comprises three sequential morphological transformations that cause swelling to increase from 0.15 to 2.5 nm. In the first two transformations, interlayer cations are replaced by hydronium ions from the solution; the third transformation involves a depolymerization and partial cross-linking of the protonated silicate sheets. The reaction of phlogopite with acidic aqueous solutions (pH 1.5–2) at high temperature ($T = 100$–140 °C) causes the nucleation of numerous monolayer etch pits on the pristine surface. Where the 2D pits recur at the same lateral position, they can accumulate to a total pit depth of up to 50 nm. The formation of an altered layer has also been detected at these conditions. The alteration affects the uppermost 4–5 layers. The layers are expanded, corrugated, highly unstable, and readily peel off the surface. Etch pit formation has been detected even underneath the altered layer. On the basis of HAFM data, dissolution rates and activation energies were calculated. The presented data show that the basal surface of phlogopite plays an important role in the dissolution process at least at elevated temperatures and that the absolute amount of released material has comparable contributions from both basal surfaces and edge surfaces.

1. Introduction

A thorough understanding of chemical weathering of silicates is impossible without profound knowledge of the mechanisms and kinetics of mineral-water interface reactions, which play a key role in weathering (e.g. Wieland et al., 1988). In this context, interface reactions of phyllosilicates have attracted particular attention because the mechanisms of alteration in aqueous solutions significantly differ from those of other rock-forming minerals (e.g. Nagy, 1995). In spite of an increasing number of studies on phyllosilicate surface reactions in aqueous solutions (e.g. Rufe and Hochella, 1999; Bosbach et al., 2000; Bickmore et al., 2001; Brandt et al., 2003), numerous questions concerning the interface reactions of phyllosilicates with aqueous solutions still remain unanswered. One important question concerns the different reactivity of basal surfaces and edge surfaces of phyllosilicates. Phyllosilicates have been assumed to preferentially dissolve from the crystal edges inward (e.g. Nagy, 1995 and references therein). In other words, the edges of sheet silicates are assumed to be much more reactive than the basal surfaces. For example, Turpault and Trotignon (1994) reported the ratio of contributions of crystal edges to basal surfaces for the corrosion of biotite to be about 250. There are some AFM studies of phyllosilicate dissolution confirming these data. Bosbach et al. (2000) and Bickmore et al. (2001) investigated dissolution of two smectites (hectorite and nontronite) under acidic conditions at room temperature, and found that these minerals dissolve preferentially at the crystal edges, whereas the basal surfaces were unreactive during the timescale of the experiment. On the other hand, microscopic experiments on chlorite basal surfaces performed by Brandt et al. (2003) showed that this mineral dissolves via the formation and spreading of shallow etch pits on the

* Corresponding author. Fax: +49 89 2180 4334.
E-mail address: guntram.jordan@lrz.uni-muenchen.de (G. Jordan).

0016-7037/$ - see front matter © 2006 Published by Elsevier Inc.
doi:10.1016/j.gca.2006.04.015

basal surface, thus indicating a layer-by-layer dissolution mechanism on the basal surface.

There are a few AFM studies describing the alteration of phlogopite and apophyllite in acidic solutions (Rufe and Hochella, 1999; Aldushin et al., 2004a,b). Rufe and Hochella (1999) pre-treated phlogopite samples in HF, in order to generate crystallographically oriented etch pits. The alteration behavior in HCl-solutions (pH 2) and distilled water (pH 5.7) was then investigated with AFM insitu experiments at room temperature. Phlogopite dissolution proceeded by removal of material from the etch pit walls; the nucleation of new etch pits was not been detected within the timeframe of the experiments (up to 127 h at pH 2). The authors further report an expansion of the topmost interlayer and the formation of an amorphous silica-enriched film due to cation leaching.

Recently, Aldushin et al. (2004a,b) used hydrothermal AFM to study the mechanism and kinetics of alteration of apophyllite [$KCa_4Si_8O_{20}(F,OH) \cdot 8H_2O$] in acidic aqueous solutions. The unique structural characteristics of this sheet silicate make it particularly interesting. Apophyllite consists of silicate layers alternating with interlayer ions (Fig. 1). The silicate layers are composed of interconnected four-membered rings, with the terminal tetrahedral apexes of the rings alternatingly pointing up and down along the *c*-direction. The terminal apexes of rings in adjoining layers oppose each other and form ≡Si–O–Ca–O–Si≡ type bonds and thus generate a kind of structural framework. Apophyllite, therefore, has many structural similarities not only to important phyllosilicates, such as micas and clays, but also to silicates with structural cages or voids like zeolites.

Under low pH conditions (pH 1.5–3, $T = 20$–100 °C, Aldushin et al., 2004a,b), the terminal oxygens of the silicate tetrahedra within the interlayer become protonated and the interlayer ions are released. Since the silicate layers of apophyllite are linked by Ca^{2+}-ions, their release causes a reduction of bonding strength between the silicate layers and an interlayer swelling. The swelling interlayer generates square shaped hillocks (3–4 Å high) on the (0 0 1) surface of apophyllite (see Fig. 2). As the swelling spreads laterally within the interlayer, the hillocks spread on the surface. The hillocks are softer than the pristine surface, and the silicate layer in the swollen area can easily be peeled off by the scanning AFM tip. Protonation and Ca-release within the next lower interlayers generates further hillocks which pile up on each other (marked by an arrow on Fig. 2a). In such a way, the reaction can proceed layer by layer into the bulk crystal (Aldushin et al., 2004a). Investigations of the reaction mechanism (Aldushin et al., 2004b) showed that the protonation and ion release within an interlayer takes place in two different sequences of individual transformations. One sequence comprises two transformation steps, the other three steps. The two-step process is morphologically marked on the surface by the transitions of pristine surface *P* into an intermediate terrace state *T* and then into the mature hillock *H* (Fig. 2a). In the three step process $P \rightarrow T \rightarrow A \rightarrow H$, the intermediate state *T* transforms into the mature hillock *H* via a re-collapsed metastable protonated state *A* which forms if two hillocks merge (Figs. 2b and c). The transformations differ in their rates and the different states significantly differ in their stabilities.

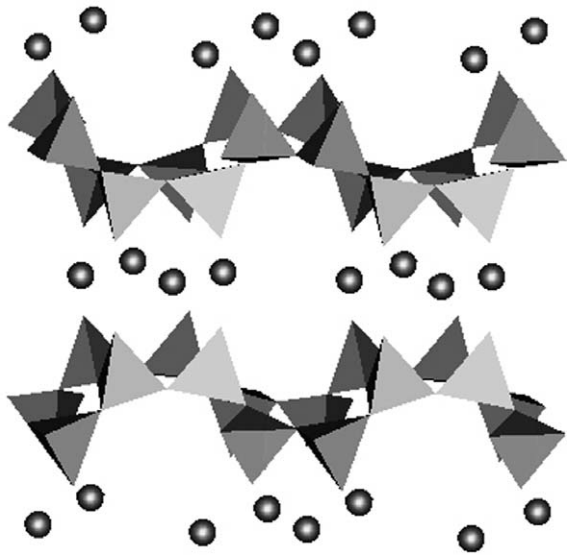

Fig. 1. Schematic structure of apophyllite: silicate rings in (0 0 1) alternatingly point up and down *c*; silica layers alternate with layers of Ca-ions (K^+, F^-, OH^- are located in the same plane and omitted for clarity, as well as H_2O molecules). The structure was created by *xtal-3D*.

While there is ample information on the mechanisms and kinetics of apophyllite alteration at strong acidic conditions (Aldushin et al., 2004a,b), little is known about the alteration of apophyllite at moderately acidic to neutral conditions. At pH 5.6 and temperatures above 110 °C, Aldushin et al. (2004a) reported dissolution via step retreat i.e., detachment of material at the steps of the silicate layers. In this study, therefore, we focus on moderate to neutral pH conditions at temperatures below 110 °C. In contrast to the acidic conditions, lower protonation and alteration rates and an enhanced stability of the reacted layers against the AFM tip can be expected. This allows for extended probing of the surface and for the possibility of detecting further alteration processes and reaction steps.

The phlogopite (0 0 1) surface was investigated at pH 1.5–2 ($T = 100$–140 °C). High temperatures significantly increase the reaction rate and allow us to skip pretreatments (such as the HF etch used by Rufe and Hochella, 1999) designed to generate reactive surface sites such as steps or pits. Thus, in situ nano-scale HAFM investigations can reveal the differences and similarities between the alteration processes of two phyllosilicate minerals and, therefore, can provide a deeper insight into the factors influencing phyllosilicate reactivity.

2. Experimental

Natural fluoroapophyllite (Poona, India; for microprobe analysis see Aldushin et al., 2004a) and phlogopite

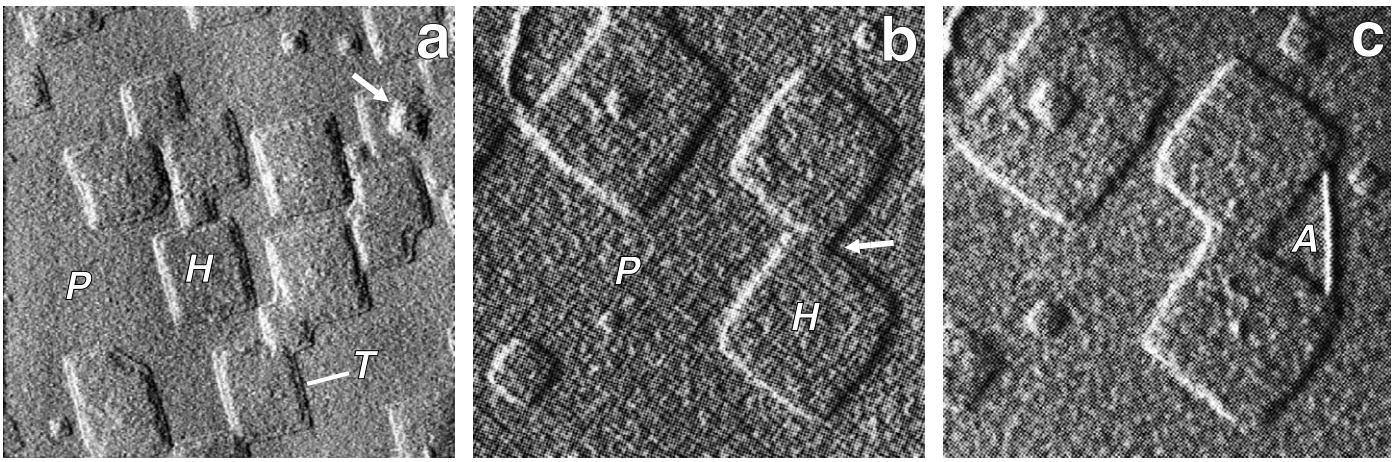

Fig. 2. Interlayer expansion generates hillocks on the pristine (0 0 1) surface of apophyllite (state *P*) at pH 2.5: (a) the expansion takes place in two steps: mature hillocks (state *H*) are surrounded by lower terraces (state *T*); the arrow marks an expansion of the second interlayer which causes a second hillock on the surface (scan field $6.2 \times 6.2\ \mu m^2$); (b) two merging hillocks; the hillocks are highly flexible, therefore the terraces (*T*) can not always be resolved by AFM; (c) 9 min after (b): in the inner corner of the hillocks (marked by an arrow in (b)) a combined terrace separates from the mature hillocks forming a conjunction between the hillocks; the conjunction progresses rapidly leaving behind a re-collapsed metastable surface area *A* which shows altered properties; scan field $0.6 \times 0.6\ \mu m^2$.

(Andranodambo, Madagaskar) were used. Electron microprobe analyses of the phlogopite yielded a chemical formula $(K_{1.95}Na_{0.05})(Mg_{5.34}Fe_{0.32}Al_{0.18}Ti_{0.06})(Si_{5.86}Al_{2.14})O_{20}(F_{3.03}OH_{0.97})$. The crystals were cleaved by a knife edge immediately before affixing them in the fluid cell by a titanium wire and immersing them in solution. The samples were 0.1–0.3 mm thick with a (0 0 1) surface area of about 15–25 mm^2. After the fluid cell had been filled with solution, the cell was closed, pressurized, and heated to the temperature of interest. The experiments ran for up to 15 h.

Solutions were prepared using high purity deionized water (resistivity: 18 MΩ cm); the pH values of solutions were adjusted to pH 1.5–5.6 at room temperature by adding HNO_3 and to pH 10 by adding NaOH. Solution flow rates through the fluid cell were varied between 0 and 10 μl/s. The volume of the cell is approximately 0.5 ml. All in situ measurements were carried out using a contact-mode hydrothermal atomic force microscope (HAFM) which was constructed in our laboratories (Higgins et al., 1998a; Jordan et al., 1999). All AFM images are presented in deflection mode (appear as illuminated from the left). Uncoated Si-cantilevers with integrated tips (spring constant: 0.1–0.3 N/m) were used.

3. Apophyllite

3.1. Results

Fig. 3a shows the apophyllite surface at pH 4 and room temperature. Initially, the hillocks which developed on the

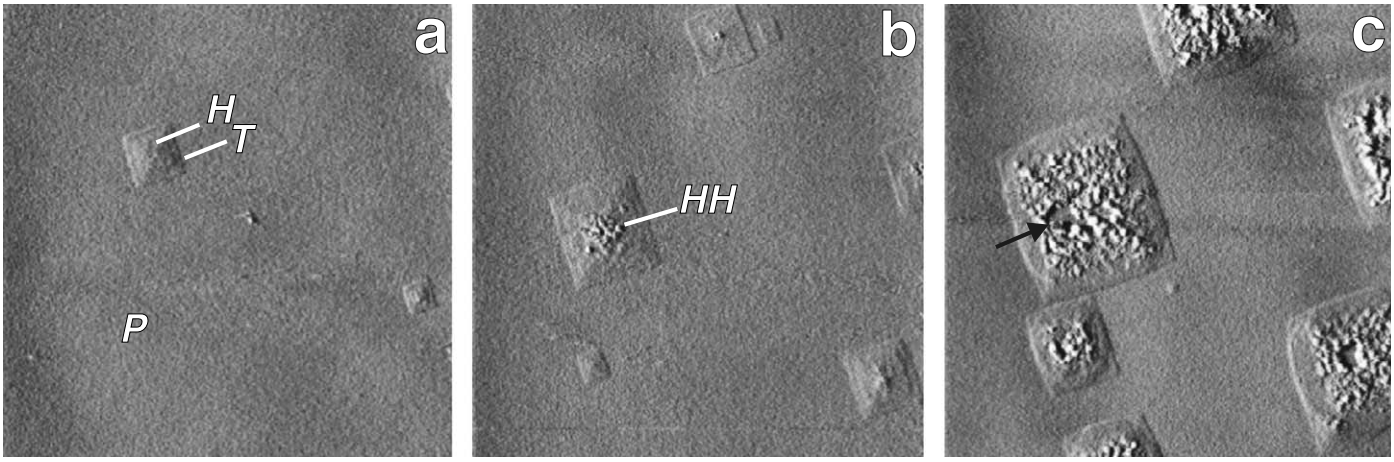

Fig. 3. Alteration on the apophyllite (0 0 1) surface at pH 4 and room temperature: (a) formation of hillocks ($P \rightarrow T \rightarrow H$ transformation); (b) 46 min later and (c) 105 min after the first image (slightly shifted): central area of the hillocks (*H*) became rough, increased in height (up to 2–3 nm), and transformed into high hillocks (*HH*); a partially peeled-off area is marked by an arrow. Scan field $2 \times 2\ \mu m^2$.

pristine surface (*P*) were similar to those obtained at pH 1.5–3 (Aldushin et al., 2004a,b). However, subsequent morphological changes indicated that at pH $\geqslant$ 4 the protonated surface in state *H* (see Section 1) undergoes further alteration. As can be seen in Fig. 3b, the central area of the hillocks (*H*) became rough and further increased in height by almost one order of magnitude (up to 2–3 nm). Thus, the hillocks eventually were transforming into another alteration state, here called *high hillocks* (*HH*). The surface in this state exhibited a higher resistance to mechanical alteration by the scanning probe in comparison to the states *H* and *T*. Although a mechanical alteration of *HH*-surface required higher loading forces of the scanning tip than in the case of state *H*, it was generally possible to partially peel off the *HH*-surface by the scanning tip (Fig. 3c, marked by an arrow). At pH 4 the transformation of apophyllite into *HH*-state was never detected without the precursor protonation of pristine surface ($P \rightarrow T \rightarrow H$ transition). Stopping the flow of pH 4 solution caused the rate of protonation reaction ($P \rightarrow T \rightarrow H$ transition) to decrease after several hours. However, the reaction $H \rightarrow HH$ advanced independently with the same rate. Thus the $H \rightarrow HH$ reaction fronts approached the $P \rightarrow T \rightarrow H$ reaction steps.

At pH values close to neutral (pH 5.6) and room temperature, little alteration was detected within several hours. Therefore, most experiments at this pH were carried out at elevated temperatures which increased the alteration rates significantly. Fig. 4 shows high hillocks (*HH*—height about 2.5 ± 0.5 nm) developing on the apophyllite surface at 50 °C. The square shaped hillocks spread slowly (4 ± 0.5 nm/min) in lateral directions, coalesced, and finally covered the surface. The $H \rightarrow HH$ transformation front follows the $P \rightarrow T \rightarrow H$ transformation front very closely so that it is difficult to resolve any reaction steps between *P* and *HH* quantitatively.

Further information about the alteration processes at the apophyllite surface was gained from pH-jump experiments. Fig. 5a shows hillocks which had been generated by protonation at pH 2.5 ($P \rightarrow T \rightarrow H$ transition) at room temperature. In situ exchange of the solution (pH 2.5 $\rightarrow$ pH 5.6) caused a deceleration of the protonation reaction and a transformation of the states *T* and *H* into *HH* (Fig. 5b). Further alteration was caused by reverse *in situ* solution exchange (pH 5.6 $\rightarrow$ pH 2.5, Figs. 5c and d). This exchange caused a recommencement of fast protonation. In Figs. 5c and d again a protonation reaction ($P \rightarrow T \rightarrow H$ transition) can be resolved that precedes the *HH* formation. Also, new hillocks developed on the pristine surface. The hillocks coalesced (indicated by arrows) and formed conjunctions and areas in state *A* (see Section 1). Another exchange of solution (pH 2.5 $\rightarrow$ pH 5.6, Fig. 5e) caused the transformation of the protonated areas (except area *A*) into the *HH*-state. A pH-jump from 5.6 to basic conditions (e.g. pH 10) caused all altered states (including area *A*) to decompose, leaving square etch pits with a depth of one half of the *c*-parameter $\sim$8 Å (Fig. 5f).

pH-jump experiments from pH 5.6 to basic pH also enabled an estimation of the vertical extent of alteration with time. The solution exchange after a prolonged treatment at pH 5.6 revealed that the alteration process was not limited to the topmost interlayers but also proceeded deeper into the crystal. Figs. 6a and b show high hillocks developing at 110 °C. The height of the hillocks reached 150 ± 20 nm. The simultaneous swelling of many layers led to warping and cracking of the hillocks. Fig. 6c shows the surface at high pH. The altered layers decomposed and large etch pits were formed on the surface with a depth up to 400 nm which corresponds to 500 altered layers. The lateral spreading velocity of the high hillocks shown in Fig. 6 was 170 ± 10 nm/min. However, the spreading rate depends on temperature (Fig. 7). Based on the data shown in Fig. 7, the activation energy for the transformation of pristine apophyllite into the altered state *HH* at pH 5.6 is 42 ± 5 kJ/mol which is close to the activation energy of 57 ± 2 kJ/mol for the $P \rightarrow T \rightarrow H$ transformation at

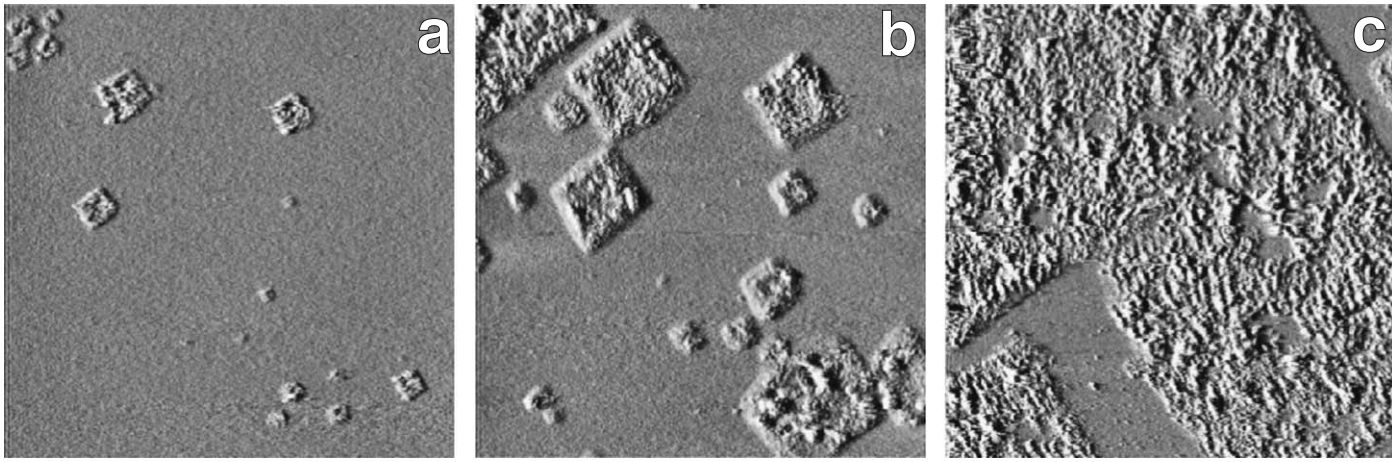

Fig. 4. Formation of state *HH* on the apophyllite surface at pH 5.6, $T = 50$ °C, $P = 9$ bar: (a) the height is about 2.5 ± 0.5 nm (the height corresponds to the average height of unpeeled hillocks with respect to the pristine surface); no rim of states *T* and *H* can be discerned; (b) 20 min and (c) 43 min after the first image: state *HH* spreads laterally and covers the surface. Scan field 1.35×1.35 μm^2.

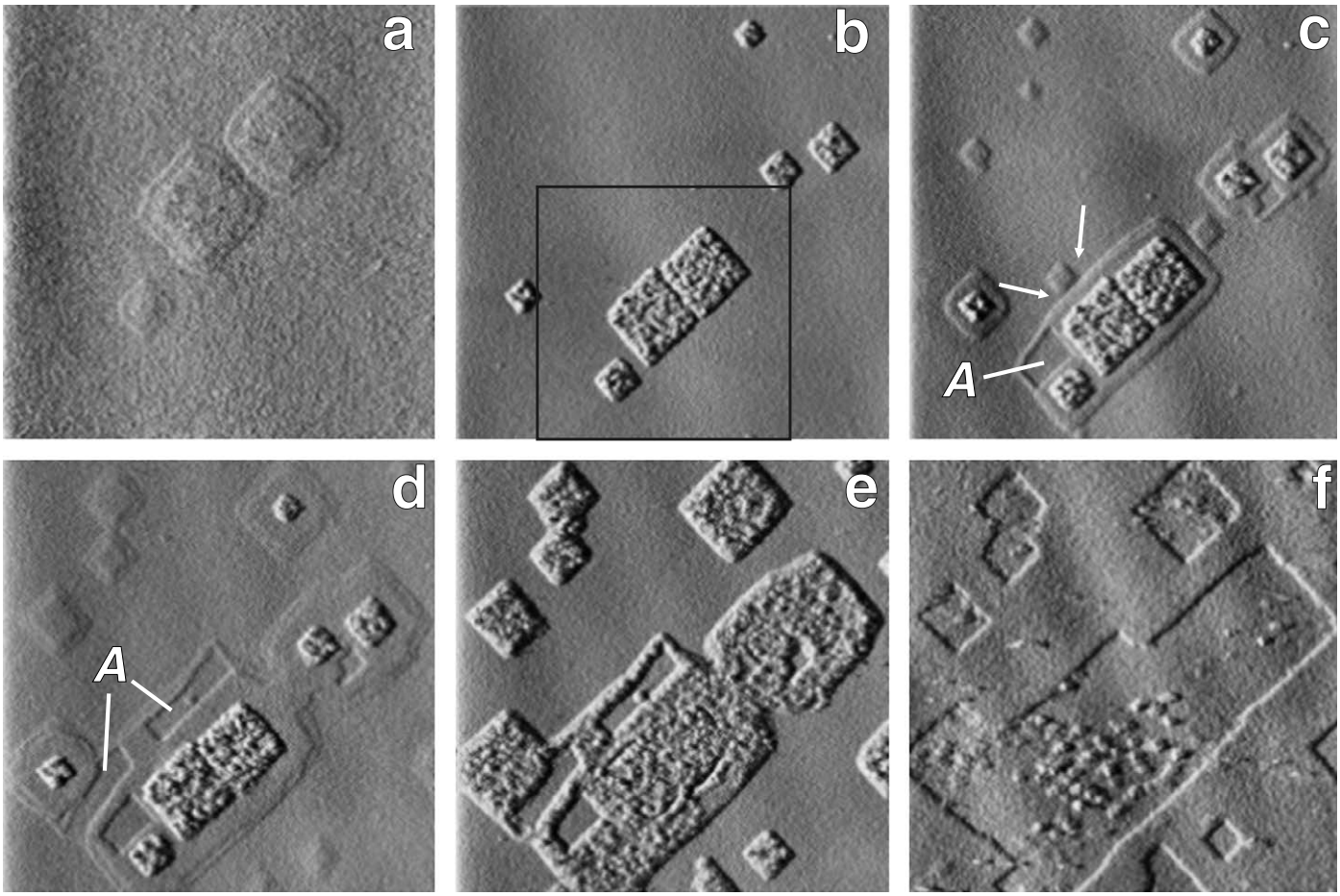

Fig. 5. In situ pH-jump experiment: pH 2.5 → pH 5.6 → pH 2.5 → pH 5.6 → pH 10 ($T = 20$ °C): (a) states T and H developed at pH 2.5 (scan field 1.7×1.7 μm^2); (b) solution exchange pH 2.5 → pH 5.6 caused states T and H to transform into high hillocks (HH) (zoom out of Fig. 4a, scan field 2.7×2.7 μm^2); (c and d) reverse solution exchange pH 5.6 → pH 2.5 caused the $P \rightarrow T \rightarrow H$ or $P \rightarrow T \rightarrow A$ reaction fronts to recommence around the state HH; arrows indicate the formation of conjunctions at coalescing hillocks; state HH remains stable within this period (about 105 min); (e) reverse solution exchange pH 2.5 → pH 5.6 caused states T and H to transform into state HH, whereas state A remained stable within this period (about 20 min); (f) solution exchange pH 5.6 → pH 10 led to the decomposition of states HH and A.

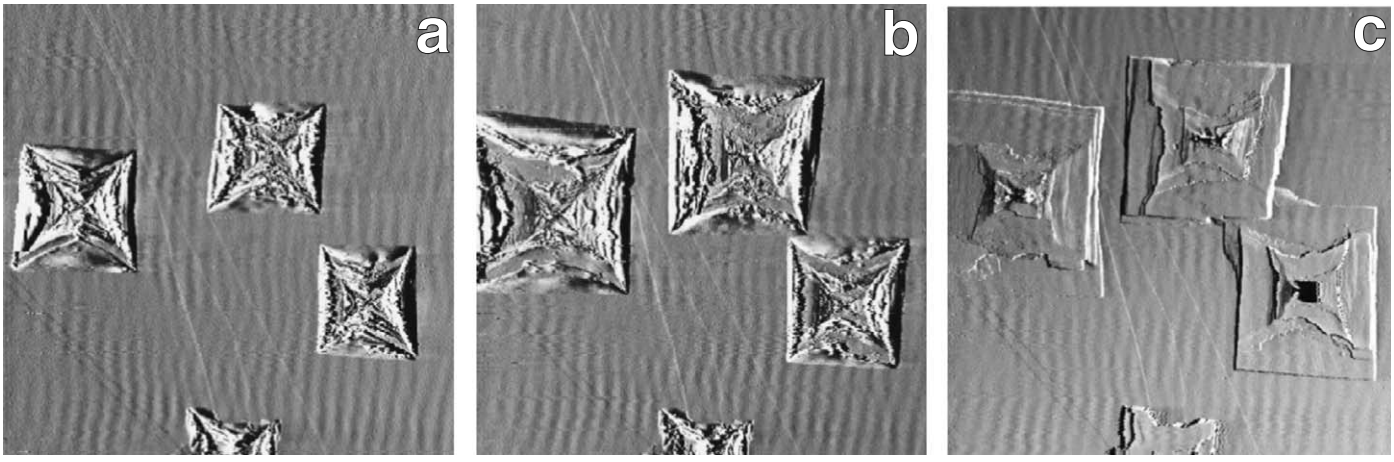

Fig. 6. Formation of state HH in multiple apophyllite layers at pH 5.6, $T = 110$ °C, $P = 7$ bar: (a) multilayer high hillocks developed at linear defects; (b) 12 min later: spreading of the hillocks; also from the cleavage steps hillocks are emanating which remain inconspicuous due to their lower height; (c) 44 min after the first image (26 min after solution exchange): solution exchange pH 5.6 → pH 10 caused the decomposition of the altered states. Scan field 35×35 μm^2.

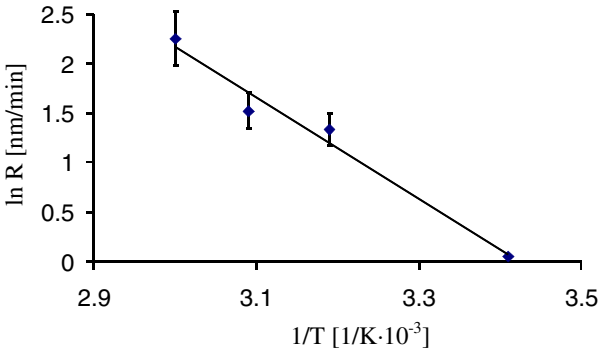

Fig. 7. Influence of temperature on the reaction rate $P \rightarrow HH$ at pH 5.6.

pH 3 (Aldushin et al., 2004b). The formation of high hillocks could be measured up to about 110 °C.

3.2. Discussion

The AFM observations on apophyllite alteration in aqueous solutions under moderate acidic conditions ($4 \leqslant pH \leqslant 5.6$) reveal: (a) the alteration reaction consists of three sequential steps: pristine surface → terrace → low hillock → high hillock ($P \rightarrow T \rightarrow H \rightarrow HH$); (b) the rate of $H \rightarrow HH$ transformation does not depend on the solution pH within the range $4 \leqslant pH \leqslant 5.6$, but increases with increasing temperature; (c) the high hillocks can be partially peeled off by the scanning tip although they are more stable than the low hillocks; (d) pH-jump from low pH (e.g. pH 2.5) to pH 5.6 causes a uniform transformation of the states T and H into HH; pH-jump from pH 5.6 to high pH (e.g. pH 10) leads to a decomposition of HH and to a formation of pits.

At pH 4 the alteration starts with the protonation of silicate layers: the pristine surface transforms via state T into the protonated state H. The protonated layers are subsequently transformed into state HH. At pH 5.6 no states T and H can be resolved by AFM, and a direct transformation of pristine surface into the HH-state was observed. The $H \rightarrow HH$ transformation rates do not depend on pH of the solution. Therefore at pH 5.6, the lower proton concentration reduces the protonation rate (i.e., the $P \rightarrow T \rightarrow H$ transformation) but not the rate of the $H \rightarrow HH$ transformation, so within the spatial resolution of the images protonation and HH formation coincide. This hypothesis is supported by the pH-jump experiments (Fig. 5). By increasing pH, the $P \rightarrow T \rightarrow H$ transformation slows down and the $H \rightarrow HH$ transition catches up with the $P \rightarrow T \rightarrow H$ transformation front. Once the two reaction fronts have bunched, they together proceed at the rate of the slower $P \rightarrow T \rightarrow H$ transformation.

According to Casey and Bunker (1990), the initial stage of silicate leaching comprises diffusion of protons and water into the bulk material, which partially hydrolyze the mineral structure and exchange alkali and alkali-earth ions. In the next stage of reaction, the silica-enriched residue may repolymerize and form a porous silica network. A similar reaction may take place in apophyllite. Two first alteration stages (T and H) are proton promoted, and represent protonation of the non-bridging tetrahedral oxygens, cation release, and separation of silica sheets (Aldushin et al., 2004b). Prolonged treatment may hydrolyze the bridging Si–O–Si bonds within the layers. In this case the $H \rightarrow HH$ transformation most probably reflects a partial depolymerization of the tetrahedral sheets followed by repolymerization in another topography. Scanning with high loading forces reveals an increased durability of the HH-area in comparison to the H-area. This further suggests a partial cross-linking between two opposing protonated silica layers probably by condensation of Si–OH groups to form siloxane (Si–O–Si) linkages. Thus high rough hillocks on the apophyllite surface can be perceived as a porous material containing water molecules within voids formed by the cross-linked silicate layers. This suggestion is supported by NMR investigations of apophyllite treated for 11 h at pH 1.6 (Aldushin et al., 2004b) which show, aside from various protonated states, the formation of $Si(OSi)_4$-type silica with variable bonding parameters.

Although the NMR results are consistent with our cross-linking and condensation proposal, there are some remaining inconsistencies that require explanation. In low pH HAFM experiments (pH 1.5–3) no transformation into the HH state was detected whereas previous work on other minerals (Jordan et al., 1999) suggest that low pH leaching leads readily to repolymerization of residual silica material. One possibility is that, because even the lowest possible loading forces caused a rapid peeling-away of the surface layers, AFM images reflect an artificially low amount of altered material that could transform into the HH material. Another possibility is that, under acidic conditions, repolymerized material forms in locations physically separate from leaching sites. In any case, Lagaly and Matouschek (1980) and Theodossiu et al. (2001) reported an amorphization of apophyllite treated in acid at room temperature. Therefore, the final product of acidic alteration of apophyllite is probably amorphous, irrespective of its location.

The results presented here contradict the results of Frondel (1979). According to this author, severe acidic treatment of apophyllite powder resulted in a poorly crystalline residue (silicic acid) but prolonged washing of the residue with H_2O caused an increasing crystallinity. The in situ pH-jump experiments indicate that the opposite process takes place: an exchange of acidic solution by pH 5.6 solution leads to an amorphization of protonated layers. The observed discrepancy may be explained by the preparation method used in the study conducted by Frondel (1979). During the prolonged washing most of the amorphous material might have been removed from the residue which may have appeared like a relative increase of crystalline material.

The AFM-observations at pH 5.6 allow us to distinguish two different morphological alteration patterns (i) hillock

development below approximately 110 °C and (ii) dissolution by detachment of material at the layers as well as spreading etch pits above this temperature. At about 110 °C, two competing processes take place: on the one hand protonation of apex oxygens and replacement of interlayer cations and on the other hand depolymerization and detachment of the silica sheet material. Above 110 °C, the attack on the Si–O–Si bonds outnumbers the proton attack on the apex oxygens. Thus, the protonation of apex oxygens, which is the key-step of high hillock formation, becomes less dominant and depolymerization of Si–O–Si bonds within the sheets becomes a more and more dominating process. Thus, the AFM-studies indicate that at close to neutral pH above 110 °C apophyllite changes its dissolution mechanism from incongruent to congruent.

4. Phlogopite

4.1. Results

The phlogopite (0 0 1) cleavage face usually is atomically flat. Steps as in Fig. 8a were observed rarely. However, the reaction of phlogopite with acidic solution at high temperature ($T = 100$ °C) caused a fast surface roughening by the nucleation of numerous randomly distributed small etch pits (Fig. 8a; mean density 40 μm^{-2}). The depth of the pits typically was about 1 or 2 nm corresponding to one or two tetrahedral-octahedral-tetrahedral (TOT)-layers in the phlogopite structure. The steps at the pits retreated laterally, coalesced, and uncovered the underlying layer. After the removal of the topmost layer, the uncovered surface started to react in the same way, i.e., by nucleation and spreading of two-dimensional pits. In addition to this randomly distributed two-dimensional pit formation, deep triangular pits were formed by an accumulation of 2D pits nucleating at the same lateral position in successive layers with high frequency (Fig. 8b). Since the nucleation frequency of these recurring 2D pits was faster than the frequency of layer removal by random 2D pit nucleation, the overall depth of the accumulated pits increased with time. Overall depths of up to 50 nm were measured. In the centre of some of these accumulated deep pits, 2D pit formation ceased with time (cf. Figs. 8c and d) transferring the accumulated pointed pyramidal etch pit into a flat-bottomed accumulated pit. The flat-bottomed accumulated pits eventually became annihilated by pit-pit coalescing. In Fig. 9 the nucleation frequency of 2D pits recurring at the same lateral position within the accumulated deep etch pits is plot-

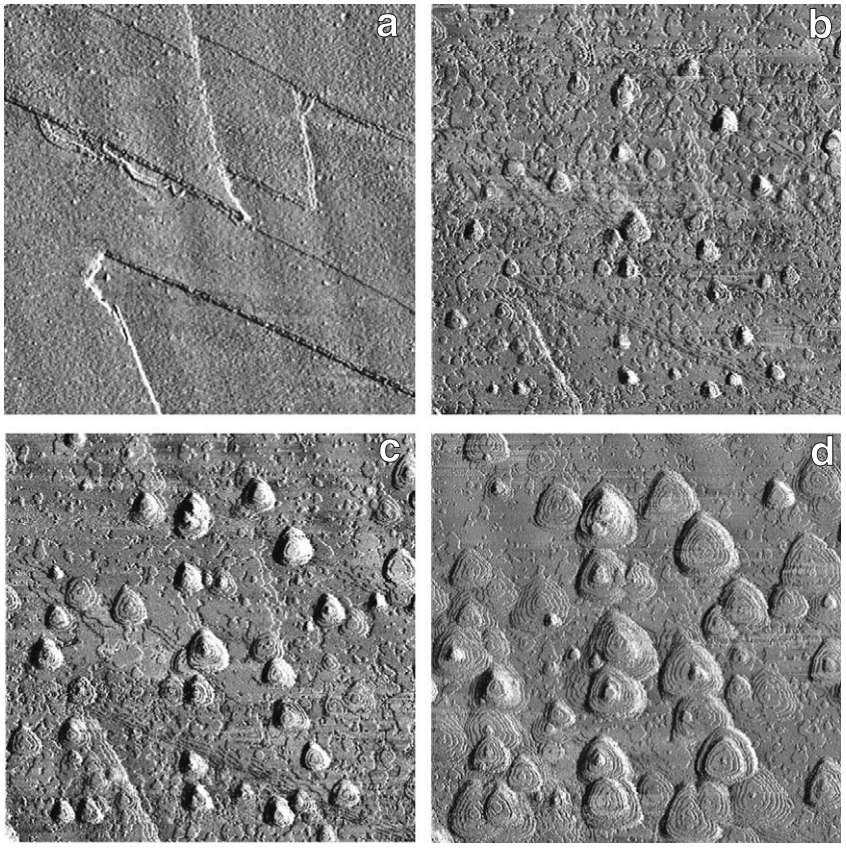

Fig. 8. Dissolution on phlogopite (001) surface at 125 °C (pH 1.8): (a) 7 min at 125 °C; the reaction of phlogopite with acidic solution caused the nucleation of numerous small etch pits; dissolution also affects cleavage steps; (b and c) 20 and 33 min later; in addition to the randomly distributed two-dimensional pit formation, deep triangular pits were formed by 2D pit nucleation recurring at the same lateral position; the cleavage steps in the upper part of the image became almost indiscernible; (d) 60 min after the first image; dissolution proceeded by nucleation and spreading of etch pits; cleavage steps are removed primarily by the coalescence with etch pits. Scan field 7×7 μm^2.

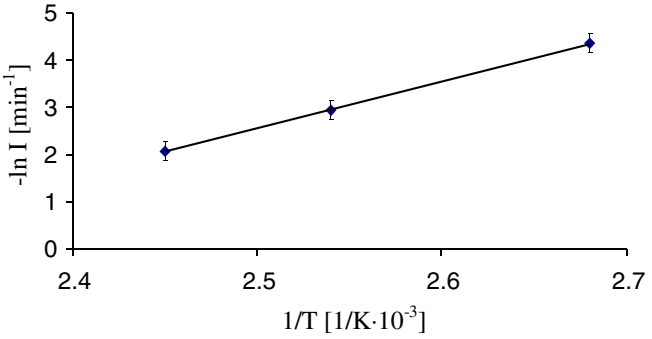

Fig. 9. Influence of temperature on the nucleation frequency of 2D pit recurring at the same lateral position within the deep etch pit at pH 2. The error bars in the diagram depict the standard deviation.

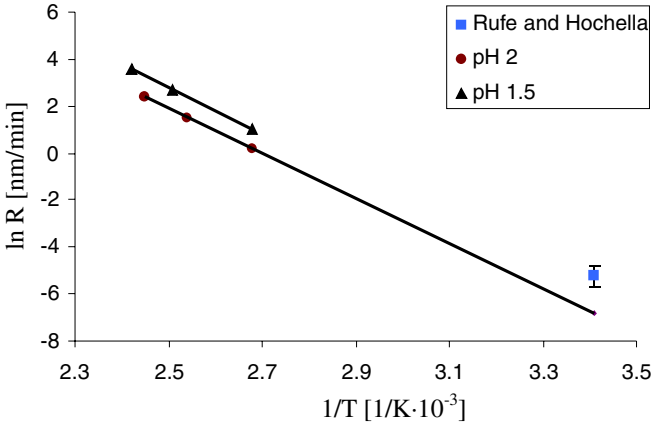

Fig. 10. Influence of temperature on the retreat rate of a monolayer step in phlogopite at pH 1.5 and pH 2. The rates presented were the initial rates of monolayer step retreat after the nucleation of pits. The data points have the size of the standard deviations. For comparison, room temperature retreat rates of phlogopite monolayer steps at pH 2 derived from Rufe and Hochella (1999) are plotted.

ted as a function of temperature at pH 2. The nucleation frequency increased from about 1/78 min^{-1} at 100 °C to about 1/8 min^{-1} at 135 °C. On the basis of these data, the activation energy of 2D pit nucleation in accumulated deep etch pits at pH 2 is 83 ± 12 kJ/mol.

Dissolution at cleavage steps consisting of just a few layers took place at the same rate as dissolution at the steps bounding the 2D etch pits. Due to rapid coalescence of the cleavage steps with those emanating from the randomly distributed 2D etch pit, the cleavage steps rapidly become irresolvable. Step bunches consisting of more than 5 layers did not retreat at a uniform rate. The steps of the upper layers retreated faster than the steps of the lower layers, causing the step bunch to spread with time. Such behavior clearly indicates step-step interaction. However, long-term observation of high cleavage steps was obstructed by the coalescence of the high cleavage steps with 2D pits (Fig. 8d). The steady state morphology eventually reached was characterized by deep accumulated 2D pits and their intersectional areas.

Fig. 10 shows the dependence of the retreat rate of a monolayer step on temperature at pH 1.5 and pH 2. Based on these data, the activation energy of step retreat on the phlogopite (0 0 1) surface at pH 1.5 and pH 2 is 78 ± 12 and 80 ± 11 kJ/mol, respectively. Note that the rates are the retreat rates of monolayer steps. The retreat rates of bunched multilayer steps were approximately half of the monolayer steps. For comparison, the retreat rate at pH 2 and 20 °C based on the data of Rufe and Hochella (1999) was inserted in Fig. 10.

On the basis of the nucleation frequencies and step retreat rates as given above, the dissolution rates for different surfaces can be calculated. Following the approach of Higgins et al. (1998b) the dissolution rate of {0 0 1} surfaces is:

$$R_{001} = x_s \cdot I$$

where x_s (mol m^{-2}) is the number of moles per m^2 of a phlogopite monolayer, and I (s^{-1}) is the nucleation frequency of 2D pits within the accumulated deep etch pits. In order to assess the dissolution kinetics at crystal edges ($\{hk0\}$ surfaces) the retreat rates of the highest observable step bunches on the (0 0 1) surface were used as a proxy for the $\{hk0\}$ surface retreat rates. The dissolution rate for $\{hk0\}$ surfaces was then calculated as:

$$R_{hk0} = x_v \cdot G$$

where x_v (mol m^{-3}) is the number of moles per m^3 phlogopite and G (m s^{-1}) is the retreat rate of step bunches consisting of at least 15 layers. x_s and x_v were calculated by the mean density and molar weight of phlogopite based on the chemical composition of the samples. The dissolution rates of phlogopite at pH 2 and different temperatures are given in Table 1.

Dissolution on the basal surface of phlogopite was accompanied by an alteration of the topmost layers. The development of altered layers requires an extended exposure of the surface to the solution. Therefore, altered layers were only observed on slowly dissolving surfaces areas with low step density. Fig. 11a shows the phlogopite surface with deep accumulated 2D pits. The central area of the image was relatively smooth and dominated by random 2D pit formation. Within this area, the uppermost 3–4 layers were affected by the alteration process. The layers expanded, corrugated, and formed a rough surface (Figs. 11b and c). The thickness of the resulting altered surface layers increased by about 50% (i.e., 5–6 nm). The altered surface layers were highly unstable and decomposed or peeled off the surface. A high tip loading force was not required in order to cause peeling. The peeling uncovered an

Table 1
Average dissolution rates of the phlogopite samples at pH 2

T (°C)	R_{001} (mol m^{-2} s^{-1})	R_{hk0} (mol m^{-2} s^{-1})
100	$7.1 \pm 0.6 \times 10^{-10}$	$3.3 \pm 0.8 \times 10^{-8}$
120	$2.8 \pm 0.6 \times 10^{-9}$	$1.1 \pm 0.3 \times 10^{-7}$
135	$7.3 \pm 2.0 \times 10^{-9}$	$3.0 \pm 0.7 \times 10^{-7}$

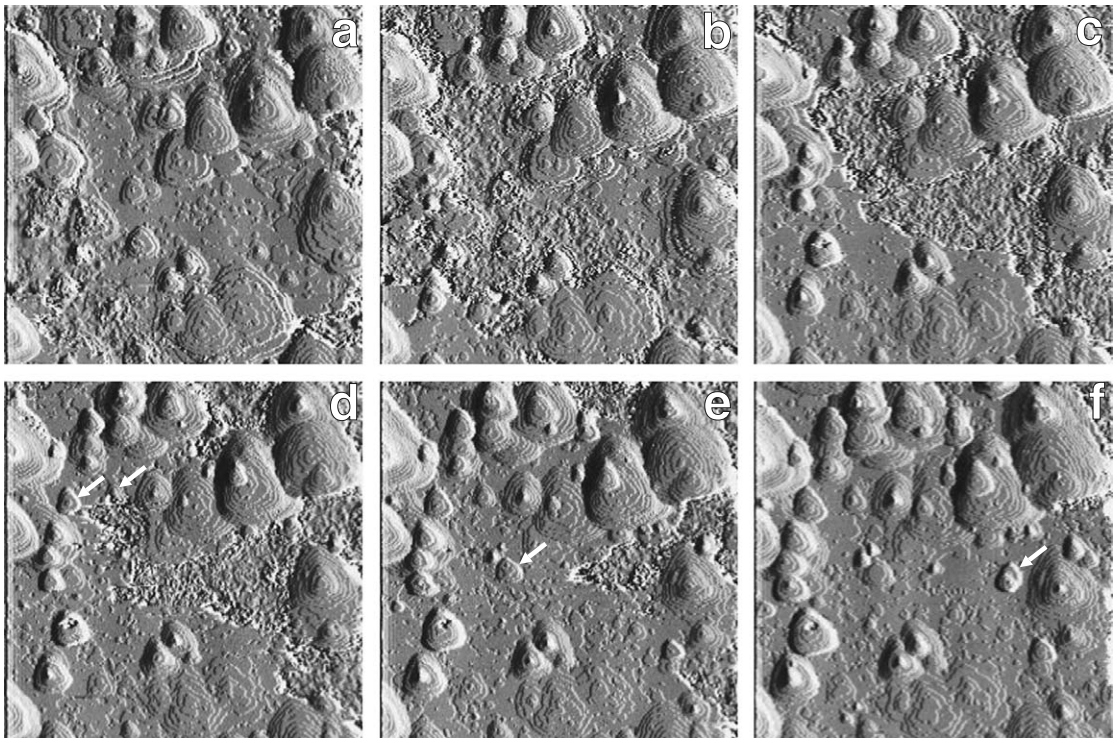

Fig. 11. Formation of altered layers on the phlogopite surface at $T = 125$ °C (pH 1.5): (a) the central area of the image is relatively smooth showing just a few 2D etch pits; (b) 8 min later: the alteration process started at the edges of deep pits and affected the uppermost 4–5 layers; the layers expanded, corrugated, and formed a rough surface; (c–e) 15, 17, and 21 min after the first image: the altered surface layers were highly unstable and readily disintegrated; arrows show etch pits which already developed underneath the altered layer; (f) 25 min after the first image: peeling of the altered layer uncovered a surface with deep etch pits. Scan field 5.5×5.5 μm^2.

underlying surface with already developed deep etch pits (Figs. 11d–f, shown by arrows). The existence of these well-developed pits indicates that their formation and spreading proceeded underneath the altered layer. Therefore, it can be suggested that the altered layer had little, if any, effect on the dissolution of the silicate layers underneath.

Fig. 12 shows the disintegration process of two successive layers in detail (left arrows mark the lower layer). The first step of the disintegration process was a layer expansion by approximately 4–5 Å taking place at a clearly resolvable reaction front (white arrows) moving from the left to the right. A few minutes later, the expanded layer corrugated and decomposed (black arrows). In contrast to the layer expansion front, the decomposition stretched across a zone of a few μm depending on the number of layers involved. The advance rate of the zone of decomposition roughly corresponded to the advance rate of the layer expansion front.

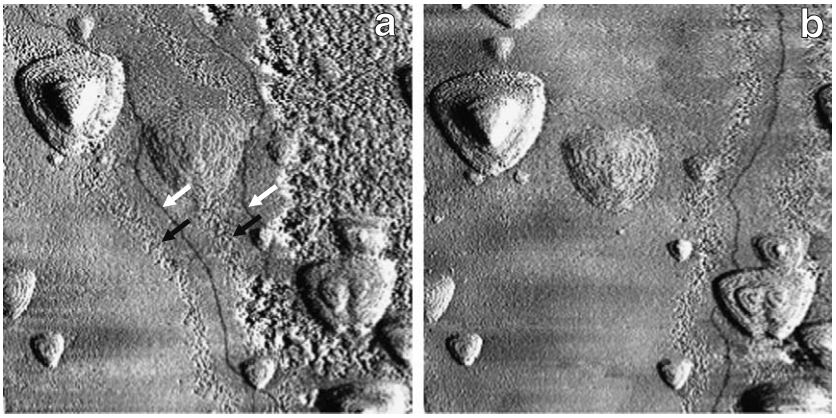

Fig. 12. Switching alteration mechanism of the phlogopite uppermost layers (pH 1.8, $T = 125$ °C): (a) scan direction—downwards: two swelling fronts (marked by white arrows) moved from left to right; after the initial swelling the surface layers decomposed (black arrows); (b) scan direction—upwards: disintegration fronts of altered layers move from left to the right side of the image (image acquisition time: 10 min, scan field 8×8 μm^2).

4.2. Discussion

Under hydrothermal conditions, the (0 0 1) phlogopite surface reacts primarily by the formation of 2D etch pits. The nucleation of 2D pits at identical lateral positions results in an accumulation of 2D pits forming deep triangular pits. This recurring nucleation at the same lateral position points towards linear defects (affecting several tens of layers) as a cause for the accumulated deep pits. Since the depth of a single 2D pit does not exceed 1–2 nm, the formation of randomly distributed 2D pits is most likely correlated to point defects. In this respect phlogopite shows some similarities to the behavior of chlorite under acidic conditions. The formation of shallow etch pits on the basal surface of chlorite was attributed to the presence of defects affecting only a single TOT or brucite-like layer (Brandt et al., 2003).

In contrast, Rufe and Hochella (1999), who studied the dissolution of phlogopite at pH 2–5.7 and room temperature, did not observe the nucleation of etch pits during their in situ experiments (i.e., the nucleation frequency I of the etch pits is close to zero), and the basal surface reacted by the formation of a leached layer and the removal of material at existing steps. According to our experiments, the 2D pit nucleation frequency I rises from approx. $2 \times 10^{-4}\,s^{-1}$ at 100 °C to approx. $2 \times 10^{-3}\,s^{-1}$ at 135 °C (pH 2). Extrapolation of these data to 20 °C yields a pit nucleation frequency of approximately $1.5 \times 10^{-7}\,s^{-1}$ which corresponds to one 2D pit in about 76 days. The duration of experiments (up to 127 h at pH 2) of Rufe and Hochella (1999) therefore was clearly not long enough to reliably determine pit nucleation frequencies as small as those derived by extrapolation from hydrothermal conditions. Thus it remains uncertain whether the nucleation frequency at room temperature is truly zero or agrees with the extrapolated value.

Fig. 10 shows an extrapolation of the step retreat rates at pH 2 from hydrothermal conditions to room temperature. Provided that the mechanism of step retreat remains unchanged, the retreat rate at room temperature is approx. $1.9 \pm 1.5 \times 10^{-3}$ nm/min. This value is within the same order of magnitude of the retreat rate derived from Rufe and Hochella (1999) at pH 2 and room temperature (approx. $5.7 \pm 2.5 \times 10^{-3}$ nm/min). Therefore, on the basis of the agreement of step retreat data it is inferred that mild hydrothermal conditions do not significantly modify the mechanism of material detachment at steps with respect to room temperature. Depending on the agreement of nucleation frequencies, this inference might be expanded to the overall dissolution mechanism. Our results, however, reveal that the increasing temperature does not generate a significantly increased thickness of a leached or altered layer and that the altered layer present at high temperatures even permits the development of etch pits underneath the layer.

At hydrothermal conditions, the layer alteration initiates at pit edges and cleavage steps and comprises swelling, roughening and decomposition. In contrast to the etch pit formation, which represents a congruent dissolution mechanism, the formation of the altered layer is most likely due to hydrolysis of the TOT-layers and preferential leaching of the cations from the interlayer and octahedral positions (Rufe and Hochella, 1999). Leaching of octahedral cations transforms the phlogopite layers into a protonated silica-enriched residue. In this respect phlogopite exhibits similarities to apophyllite which also forms an amorphous silica-enriched residue at acidic conditions. The amorphization of the phlogopite surface is preceded by swelling (Fig. 12d), which is also analogues to apophyllite alteration. However, the formation of the altered layer was observed in only 20% of the experiments. The formation of this layer probably requires an extended exposure of the surface to the solution and may in addition require specific compositional or structural conditions or defects.

The formation of the leached layer on phlogopite observed here is consistent with the data presented by Kaviratna and Pinnavaia (1994). They investigated the products of phlogopite and fluorohectorite alteration under acidic treatments. According to their data, acidic treatment of phlogopite involves a separation of TOT-layers that allows protons and water to penetrate between the tetrahedral sheets; a subsequent cross-linking of the solvated sheets causes a formation of amorphous residue. These authors suggest two possible mechanisms of phyllosilicate alteration: the edge attack (proton attack at the edges of the layers) and the gallery access mechanism (cation leaching through the ditrigonal cavities of the basal surface). According to their data the acid hydrolysis of phlogopite occurs primarily by the edge attack mechanism.

The alteration process is completed by the decomposition of the altered layers. This result differs from Rufe and Hochella (1999). These authors observed changes in thickness of the top layer during the acidic treatment of phlogopite. The observed changes were explained by depolymerization (layer expansion) and repolymerization (layer contraction) reactions occurring during leached layer formation. However, under hydrothermal conditions a contraction of depolymerized layers was not observed. The leached layer obviously is highly unstable at hydrothermal acidic conditions, readily disintegrates, and uncovers the underlying surface. Applying various scanning parameters allows to assume that the influence of the scanning tip to the disintegration can be neglected.

AFM permits no access to crystal edges (i.e., $\{hk0\}$ faces) but allows observation of the behavior of cleavage steps and steps at etch pits on the (0 0 1) surface. While the height of cleavage steps is up to 20 nm, the thickness of uniform facets at the crystal edges may reach up to 50 μm. Therefore, the reactions at step sites may be influenced by the basal surface to some extent. Nevertheless, some information about the crystal edges can be inferred from steps on the (0 0 1) surface. Here we calculated the dissolution rates for different surfaces on the basis of the kinematics of the basal surface. According to these data, the dissolution rate

on the crystal edge surfaces $\{hk0\}$ is about 30–40 times faster than on the basal surfaces. The dissolution rates of the $\{hk0\}$ and $\{001\}$ surfaces represent boundary values for the overall dissolution rate of phlogopite. The actual overall rate depends on the ratio of the surface areas of $\{hk0\}$ and $\{001\}$. For the crystals used, the ratio $S\{001\}/S\{hk0\}$ was about 15–20. Fig. 13 shows the dependence of the overall rates on the surface area ratio. At $S\{001\}/S\{hk0\} = 10$ the overall dissolution rate is considerably influenced by $R\{001\}$, and at $S\{001\}/S\{hk0\} = 50$ the rate is close to $R\{001\}$. Thus, the dissolution rate of phlogopite is significantly affected by the reactivity of the basal surface. Furthermore, the contributions of the different types of surfaces to the amount of dissolved material are comparable.

Fig. 13 also shows the extrapolation of the dissolution rates to room temperature and the data reported by Kalinowski and Schweda (1996) and Rufe and Hochella (1999). The rate of Kalinowski and Schweda (1996) agrees very well with the extrapolated data. Also, the overall rate of Rufe and Hochella (Fig. 13, R&H tot) lies well within the boundary values $R\{001\}$ and $R\{hk0\}$. However, R&H (tot) is based on time dependent ratios $S\{001\}/S\{hk0\}$ ranging from 20 to 206 with an average of 110. For comparison, the overall rate with a basal/edge ratio of 110 based on our data lies very close to the $R\{001\}$ value.

The rate of Rufe and Hochella (1999) normalized to the edge surface area (Fig. 13, $R\&H\{hk0\}$) is considerably higher than the upper boundary value obtained by extrapolation. This discrepancy results from two points. First, Rufe and Hochella (1999) used monolayer steps for deriving the dissolution rates whereas the data presented here are based on the retreat rate of step bunches. Second, the monolayer step retreat rates reported by Rufe and Hochella (1999) are higher than the monolayer retreat rates extrapolated from our data (Fig. 10).

5. Conclusion

The results clearly show both differences and similarities in the kinetics and pathways of apophyllite and phlogopite alteration. The dissolution rate of phlogopite at room temperature and pH 2 is about 10^{-11} mol m^{-2} s^{-1} (Kalinowski and Schweda, 1996; Rufe and Hochella, 1999). However, under hydrothermal conditions phlogopite reacts readily and shows a cascade of alteration mechanisms. In contrast, the alteration of apophyllite is easily detectable by AFM even at room temperature and pH 4.

Further differences in alteration of phlogopite and apophyllite can be linked to structural differences. The silicate layers in apophyllite consist of single sheets of $[SiO_4]$-tetrahedra, which are bonded by Ca-ions. Therefore, a replacement of interlayer Ca^{2+} by H_3O^+ causes a protonation of the non-bridging oxygens of the silicate layers and a subsequent swelling of the layers. In phlogopite, non-bridging oxygens are located within the TOT layers and are less accessible. Therefore, Si–O–Si bonds in protonated apophyllite layers are highly receptive to further attack, whereas strong acidic treatment is needed for the disruption of bonds within the phlogopite TOT-layer.

Nevertheless, irrespective of the different extent of swelling, both minerals form an expanded leached layer. However, the vertical expansion of the leached layer on apophyllite is larger than on phlogopite. A similar discrepancy has been reported for phlogopite and fluorohectorite (Kaviratna and Pinnavaia, 1994). Both minerals have been found to react similarly but the surface area of hydrolysis product of fluorohectorite was about 7.5 times greater than the surface area of the phlogopite-derived residue, thus indicating different swelling characteristics.

Under high temperature conditions the formation of etch pits has been observed on both apophyllite and phlogopite surfaces. On apophyllite, dissolution via etch pit for-

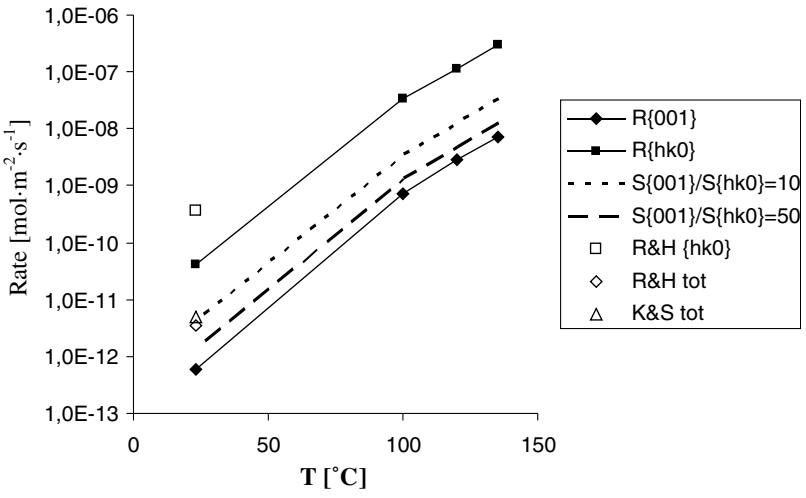

Fig. 13. Surface dependent phlogopite dissolution rates. $\{hk0\}$ faces and $\{001\}$ faces mark boundary reactivities. Rates of different ratios of surface areas ($S\{001\}/S\{hk0\} = 10$ and $S\{001\}/S\{hk0\} = 50$) are included. The HAFM data were extrapolated to room temperature. Room temperature rates of Kalinowski and Schweda (1996) and Rufe and Hochella (1999) are inserted.

mation occurs above approximately 110 °C at pH 4–5.6, whereas below this temperature apophyllite reacts via the formation of an amorphous expanded layer. The dominating alteration mechanism of apophyllite, therefore, changes with temperature. Due to the low reactivity of phlogopite at room temperature, there is little information about a change in dissolution mechanism. Nevertheless, the kinetic data show that the phlogopite dissolution rate is clearly influenced by the reactivity of the basal surface and that the absolute amount of released material has comparable contributions from both basal surfaces and edge surfaces. Thus, the contributions of the basal surfaces of phyllosilicates to alteration and dissolution in aqueous solutions might generally be underestimated at least at elevated temperatures.

Acknowledgments

The authors thank Heinz-Jürgen Bernhardt and Hans-Peter Schertl (Ruhr-Universität Bochum) for performing the EPM analysis and for providing excellent phlogopite samples. Funding of this project has been provided by the Deutsche Forschungsgemeinschaft and is gratefully acknowledged. Furthermore, the authors are grateful to Associated Editor Carrick M. Eggleston for editorial handling and improving the manuscript and to three anonymous reviewers for helpful comments.

Associate editor: Carrick M. Eggleston

References

Aldushin, K., Jordan, G., Rammensee, W., Schmahl, W.W., Becker, H.-W., 2004a. Apophyllite (0 0 1) surface alteration in aqueous solutions studied by HAFM. *Geochim. Cosmochim. Acta* **68**, 217–226.

Aldushin, K., Jordan, G., Fechtelkord, M., Schmahl, W.W., Becker, H.-W., Rammensee, W., 2004b. On the mechanism of apophyllite alteration in aqueous solutions. A combined AFM, XPS and MAS NMR study. *Clays & Clay Miner.* **52**, 432–442.

Bickmore, B.R., Bosbach, D., Hochella Jr., M.F., Charlet, L., Rufe, E., 2001. In situ atomic force microscopy study of hectorite and nontronite dissolution: implications for phyllosilicate edge surface structures and dissolution mechanisms. *Amer. Mineral.* **86**, 411–423.

Bosbach, D., Charlet, L., Bickmore, B., Hochella Jr., M.F., 2000. The dissolution of hectorite: In-situ, real-time observations using atomic force microscopy. *Amer. Mineral.* **85**, 1209–1216.

Brandt, F., Bosbach, D., Krawczyk-Barsch, E., Arnold, T., Bernhard, G., 2003. Chlorite dissolution in the acid pH-range: a combined microscopic and macroscopic approach. *Geochim. Cosmochim. Acta* **67**, 1451–1461.

Casey, W.H., Bunker, B.C. 1990 The leaching of mineral and glass surfaces during dissolution. In: Hochella Jr., M.F. and White, A. (Eds.), Reviews in Mineralogy: Mineral-Water Interface Geochemistry 22, 397–426.

Frondel, C., 1979. Crystalline silica hydrates from leached silicates. *Amer. Mineral.* **64**, 799–804.

Higgins, S.R., Eggleston, C.M., Knauss, K.G., Boro, C.O., 1998a. A hydrothermal atomic force microscope for imaging in aqueous solution up to 150 °C. *Rev. Sci. Instrum.* **69**, 2994–2998.

Higgins, S.R., Jordan, G., Eggleston, C.M., Knauss, K.G., 1998b. Dissolution kinetics of the barium sulfate (0 0 1) surface by hydrothermal atomic force microscopy. *Langmuir* **14**, 4967–4971.

Jordan, G., Higgins, S.R., Eggleston, C.M., Swapp, S.M., Janney, D.E., Knauss, K.G., 1999. Acidic dissolution of plagioclase: in-situ observations by hydrothermal atomic force microscopy. *Geochim. Cosmochim. Acta* **63**, 3183–3191.

Kalinowski, B.E., Schweda, P., 1996. Kinetics of muscovite, phlogopite, and biotite dissolution and alteration at pH 1–4, room temperature. *Geochim. Cosmochim. Acta* **60**, 367–385.

Kaviratna, H., Pinnavaia, T.J., 1994. Acid hydrolysis of octahedral Mg^{2+} sites in 2:1 layered silicates: an assessment of edge attack and gallery access mechanisms. *Clays & Clay Miner.* **42**, 717–723.

Lagaly, G., Matouschek, R., 1980. The crystalline silicic acids from apophyllite, carletonite and gillespite. *N. Jb. Mineral. / Abh.* **138**, 81–93.

Nagy, K.L., 1995. Dissolution and precipitation kinetics of sheet silicates. In: White, A.F., Brantley, S.L. (Eds.), *Chemical Weathering Rates of Silicate Minerals*, Vol. 31. Mineralogical Society of America, pp. 173–233.

Rufe, E., Hochella Jr., M.F., 1999. Quantitative assessment of reactive surface area of phlogopite during acid dissolution. *Science* **285**, 874–876.

Theodossiu, W., Misaelides, P., Godelitsas, A., 2001. Investigation of fluorine distribution on the surface of acid-treated apatite single crystals using nuclear resonant reaction analysis. *Cryst. Res. Technol.* **36**, 1247–1251.

Turpault, M.-P., Trotignon, L., 1994. The dissolution of biotite single crystals in dilute HNO_3 at 24 °C: evidence of an anisotropic corrosion process of micas in acidic solutions. *Geochim. Cosmochim. Acta* **58**, 2761–2775.

Wieland, E., Wehrli, B., Stumm, W., 1988. The coordination chemistry of weathering: III. A generalization on the dissolution rates of minerals. *Geochim. Cosmochim. Acta* **52**, 1969–1981.